Insight into Global Trends in Aerosol Composition over 2005-2015 Inferred from the OMI Ultraviolet Aerosol Index

Melanie S. Hammer[1], Randall V. Martin[1,2], Chi Li[1], Omar Torres[3], Max Manning[1], Brian L. Boys[1]

[1]Department of Physics and Atmospheric Science, Dalhousie University, Canada

[2]Harvard-Smithsonian Center for Astrophysics, Cambridge, MA, USA

[3]Atmospheric Chemistry and Dynamics Laboratory, NASA Goddard Space Flight Center, Greenbelt, MD, 20770, USA

Correspondence: melanie.hammer@dal.ca

Abstract

Observations of aerosol scattering and absorption offer valuable information about aerosol composition. We apply a simulation of the Ultraviolet Aerosol Index (UVAI), a method of detecting aerosol absorption from satellite observations, to interpret UVAI values observed by the Ozone Monitoring Instrument (OMI) over 2005-2015 to understand global trends in aerosol composition. We conduct our simulation using the vector radiative transfer model VLIDORT with aerosol fields from the global chemical transport model GEOS-Chem. We examine the 2005-2015 trends in individual aerosol species from GEOS-Chem, and apply these trends to the UVAI simulation to calculate the change in simulated UVAI due to the trends in individual aerosol species. We find that global trends in the UVAI are largely explained by trends in absorption by mineral dust, absorption by brown carbon, and scattering by secondary inorganic aerosol. Trends in absorption by mineral dust dominate the simulated UVAI trends over North Africa, the Middle-East, East Asia, and Australia. The UVAI simulation well resolves observed negative UVAI trends over Australia, but underestimates positive UVAI trends over North Africa and Central Asia near the Aral Sea, and underestimates negative UVAI trends over East Asia. We find evidence of an increasing dust source from the desiccating Aral Sea, that may not be well represented by the current generation of models. Trends in absorption by brown carbon dominate the simulated UVAI trends over biomass burning regions. The UVAI simulation reproduces observed negative trends over central South America and West Africa, but underestimates observed UVAI trends over boreal forests. Trends in scattering by secondary inorganic aerosol dominate the simulated UVAI

32   trends over the eastern United States and eastern India. The UVAI simulation slightly

33   overestimates the observed positive UVAI trends over the eastern United States, and

34   underestimates the observed negative UVAI trends over India. Quantitative simulation of the OMI

35   UVAI offers new insight into global trends in aerosol composition.

36

37   **1. Introduction**

38   Atmospheric aerosols have significant climate impacts due to their ability to scatter and

39   absorb solar radiation and to their indirect effect through modification of cloud properties. The

40   exact magnitude of the direct radiative forcing remains highly uncertain (IPCC, 2014), although

41   most studies agree it is significant (Andreae and Gelencsér, 2006; Mann and Emanuel, 2006;

42   Mauritsen, 2016). Storelvmo et al. (2016) estimate that changes in global aerosol loading over the

43   past 45 years have caused cooling (direct and indirect) that masks about one third of the

44   atmospheric warming due to increasing greenhouse gas emissions. Aerosol absorption has been

45   estimated to be the second largest source of atmospheric warming after carbon dioxide

46   (Ramanathan and Carmichael, 2008; Bond et al., 2013; IPCC, 2014), although considerable

47   uncertainty remains regarding the exact magnitude (Stier et al., 2007). The large uncertainty

48   regarding the direct radiative impacts of aerosols on climate is driven by the large variability in

49   aerosol physical and chemical properties, as well as their various emission sources, making it

50   extremely difficult to fully understand their interactions with radiation (Pöschl, 2005; Moosmüller

51   et al., 2009; Curci et al., 2015; Kristiansen et al., 2016). Global observations of trends in aerosol

52   scattering and absorption would offer valuable constraints on trends in aerosol sources and

53   composition.

54   The emissions of aerosols and their precursors have changed significantly over the past

55   decade. In North America and Europe, the anthropogenic emissions of most aerosol species (e.g.

56   black carbon, organic aerosols) and aerosol precursors (e.g. sulfur dioxide and nitrogen oxides)

57   have decreased due to pollution controls (Leibensperger et al., 2012; Klimont et al., 2013; Curier

58   et al., 2014; Simon et al., 2014; Xing et al., 2015; Li et al., 2017a). By contrast, emissions of

59   aerosols and aerosol precursors have increased in developing countries due to increased industrial

60   activity, particularly in China and India. Chinese emissions of black carbon (BC), organic carbon

61   (OC), and nitrogen oxides (NO_x) have been increasing over the past decade (Zhao et al., 2013; Cui

62   et al., 2015), although in the most recent years NO_x emissions have been declining, driven by

63 denitration devices at power plants (Liu et al., 2016). Due to the wide implementation of flue-gas

64 desulfurization equipment on most power plants in China, emissions of sulfur dioxide (SO_2) in

65 some regions have been decreasing since about 2006-2008 (Lu et al., 2011; Wang et al., 2015;

66 Fioletov et al., 2016). Indian emissions of anthropogenic aerosols and their precursors have been

67 increasing over the past decade (Lu et al., 2011; Klimont et al., 2017). There have also been

68 significant changes in global dust and biomass burning emissions. Shao et al. (2013) use synoptic

69 data to estimate a global decrease in dust emissions between 1974 and 2012, driven largely by

70 reductions from North Africa with weaker contributions from Northeast Asia, South America, and

71 South Africa. By examining trends in burned area, Giglio et al. (2013) estimate a decrease in global

72 biomass burning emissions between 2000 and 2012. Trends in aerosol composition produced by

73 these changing emissions may be detectable from satellite observations of aerosol scattering and

74 absorption.

75   Detection of aerosol composition from passive nadir satellite observations is exceedingly

76 difficult; few methods exist. The aerosol-type classification provided by retrievals from the MISR

77 instrument, enabled by multi-angle viewing, is one such source of information about aerosol

78 composition from constraints on particle size, shape, and single scattering albedo (SSA) (Kahn

79 and Gaitley, 2015). MISR retrievals have been used to classify particles relating to events such as

80 biomass burning, desert dust, volcanic eruptions, and pollution events (e.g. Liu et al., 2007;

81 Kalashnikova and Kahn, 2008; Dey and Di Girolamo, 2011; Scollo et al., 2012; Guo et al., 2013).

82 The most commonly used satellite product for aerosol information is aerosol optical depth (AOD),

83 the columnar extinction of radiation by atmospheric aerosols. AOD can be retrieved from satellite

84 measurements of top of atmosphere radiance in combination with prior knowledge of aerosol

85 optical properties. Several studies have examined trends in satellite AOD. Following trends in

86 emissions, over the past decade positive trends in satellite AOD have been observed over Asia and

87 Africa corresponding to regions experiencing industrial growth (de Meij et al., 2012; Chin et al.,

88 2014a; Mao et al., 2014; Mehta et al., 2016), while negative trends in satellite AOD have been

89 observed over North America and Europe, largely due to pollution controls (Hsu et al., 2012; de

90 Meij et al., 2012; Chin et al., 2014b; Mehta et al., 2016). Studies such as these demonstrate the

91 information about the evolution of aerosol abundance offered by total column AOD retrievals,

92 however measurements of absorption would complement the scattering information in AOD

93 retrievals by providing independent information on aerosol composition.

94   The Ultraviolet Aerosol Index (UVAI) is a method of detecting aerosol absorption from
95 satellite measured radiances (Herman et al., 1997; Torres et al., 1998). Because the UVAI is
96 calculated from measured radiances, a priori assumptions about aerosol composition are not
97 required for its calculation, thus yielding independent information on aerosol scattering (Herman
98 et al., 1997; Torres et al., 1998, 2007; de Graaf et al., 2005; Penning de Vries et al., 2009) and
99 absorption. The UVAI has been widely applied to examine mineral dust (Israelevich et al., 2002;
100 Schepanski et al., 2007; Badarinath et al., 2010; Huang et al., 2010) and biomass burning aerosols
101 (Duncan et al., 2003; Guan et al., 2010; Torres et al., 2010; Kaskaoutis et al., 2011; Mielonen et
102 al., 2012), including brown carbon (Jethva and Torres, 2011; Hammer et al., 2016). The UVAI is
103 not typically used to examine scattering aerosol, however aerosol scattering causes a net decrease
104 in the overall value of the UVAI, meaning that the UVAI could be used to detect changes due to
105 both aerosol absorption and scattering. Prior interpretation of the UVAI has been complicated by
106 its dependence on geophysical parameters, such as aerosol layer height (Herman et al., 1997;
107 Torres et al., 1998; de Graaf et al., 2005). Examining trends in the UVAI would provide an exciting
108 opportunity to investigate the evolution of aerosol absorption and scattering over time, if the
109 multiple parameters affecting the UVAI could be accounted for through simulation.

110   In this work, we apply a simulation of the UVAI, which was developed and evaluated
111 regionally and seasonally in Hammer et al. (2016), to interpret trends in recently reprocessed OMI
112 UVAI observations for 2005-2015 to understand global changes in aerosol composition. We
113 interpret observed UVAI values by using a radiative transfer model (VLIDORT) to calculate
114 UVAI values as a function of simulated aerosol composition from the global 3-D chemical
115 transport model GEOS-Chem. Comparison of trends in observed OMI UVAI values to the trends
116 in simulated UVAI values, which are calculated using known aerosol composition, enables
117 qualification of how changes in aerosol absorption and scattering could influence the observed
118 UVAI trends and identification of model development needs. We conduct our analysis at the global
119 scale to understand trends worldwide. Section 2 describes the OMI UVAI observations and our
120 UVAI simulation. Section 3 examines the trends in emissions of GEOS-Chem aerosols and their
121 precursors for 2005-2015 to provide context for the trends in our simulated UVAI. Section 4
122 compares the mean values over 2005-2015 of the OMI UVAI and our simulated UVAI. Section 5
123 compares the 2005-2015 trends in OMI and simulated UVAI values. In section 6 we examine the
124 sensitivity of the UVAI to changes in the abundance of individual aerosol species. Trends in our

125 UVAI simulation are interpreted by applying the trends in the GEOS-Chem aerosol species to

126 calculate the associated change in UVAI. Section 7 reports the conclusions.

127

128 **2. Methods**

129 **2.1 OMI Ultraviolet Aerosol Index**

130   The OMI Ultraviolet Aerosol Index is a method of detecting absorbing aerosols from

131 satellite measurements in the near-UV wavelength region and is a product of the OMI Near-UV

132 algorithm (OMAERUV) (Herman et al., 1997; Torres et al., 1998, 2007). The OMAERUV

133 algorithm uses the 354 nm and 388 nm radiances measured by OMI to calculate the UVAI as a

134 measure of the deviation from a purely Rayleigh scattering atmosphere bounded by a Lambertian

135 reflecting surface. Positive UVAI values indicate absorbing aerosol while negative values indicate

136 non-absorbing aerosol. Near-zero values occur when clouds and Rayleigh scattering dominate.

137 Negative UVAI values due to aerosol scattering are often weak and have historically been affected

138 by noise in previous datasets (Torres et al., 2007; Penning de Vries et al., 2015). Because UVAI

139 values are calculated from top of atmosphere (TOA) radiance which contains total aerosol effects,

140 the presence (or lack) of scattering aerosol along with absorbing aerosol can either weaken (or

141 strengthen) the absorption signal. Therefore the UVAI could be used to detect changes over time

142 due to both aerosol absorption and scattering.

143   In this analysis, we carefully address UVAI error sources to enable quantitative analysis of

144 long term trends. We use a recently reprocessed version of the UVAI algorithm which treats clouds

145 with a Mie-scattering based water cloud model (Torres et al., 2018). This new dataset more

146 accurately accounts for scattering by mineral dust and by clouds, reducing systematic artifacts and

147 scan angle bias. We focus on cloud-filtered observations by excluding scenes with OMI UVAI

148 radiative cloud fraction exceeding 5% to further reduce uncertainty due to clouds. Since 2008 the

149 OMI observations have been affected by a row anomaly which reduces the sensor viewing

150 capability for specific scan angles (http://projects.knmi.nl/omi/research/product/rowanomaly-

151 background.php). The sudden suppression of observations for specific viewing geometries (i.e. the

152 row anomaly), could cause an additional spurious trend in the UVAI calculation. We reduce this

153 concern by using the recently reprocessed OMAERUV UVAI that is less sensitive to scan-angle

154 dependent cloud artifacts and by considering only scan positions 3-23 which remain unaffected by

155 the row anomaly. The monthly time series data are deseasonalized by subtracting the monthly

156 mean for the period 2005-2015 to focus on the long-term trend. Prior to regression, the data is

157 aggregated to monthly mean values, and each pixel is required to have data for at least 60% of the

158 time period in order for regression to be performed. We perform trend analysis on monthly mean

159 time series data for the years 2005-2015 using Generalized Least Squares (GLS) regression, as

160 described by Boys et al. (2014). An additional small, positive, spurious trend in the cloud-filtered

161 OMI UVAI remains which is believed to be due to instrumental effects (Torres et al., 2017). We

162 subtract this spurious global mean trend in the cloud-filtered UVAI prior to interpretation. In the

163 following section, we discuss our UVAI simulation and the implementation of the new UVAI

164 algorithm in the simulation.

165

166 **2.2 Simulated UVAI**

167   We simulate the UVAI using the VLIDORT radiative transfer model (Spurr, 2006),

168 following Buchard et al. (2015) and Hammer et al. (2016). We calculate the top of atmosphere

169 radiances at 354 nm and 388 nm needed for the UVAI calculation by supplying VLIDORT with

170 the OMI viewing geometry for each scene, as well as the GEOS-Chem simulation of vertical

171 profiles of aerosol extinction, spectrally dependent single scattering albedo, and the corresponding

172 spectrally dependent scattering phase function. Thus these parameters account for the sensitivity

173 of the UVAI to aerosol layer height and spectrally dependent aerosol optical properties.

174   We introduce to the UVAI simulation a Mie-scattering based water cloud model

175 (Deirmendjian, 1964) for consistency with the reprocessed OMI UVAI dataset. Following Torres

176 et al. (2018), we compute the radiances used in the UVAI calculation as a combination of clear

177 and cloudy sky conditions. We use the same cloud fractions and cloud optical depths used in the

178 OMI UVAI algorithm for coincident OMI pixels. We avoid cloudy scenes by considering only

179 pixels with OMI radiative cloud fraction of less than 5%. For the UVAI calculation we use the

180 surface reflectance fields provided by OMI. We calculated the 2005-2015 trends in these surface

181 reflectance fields, and found that they were statistically insignificant globally and on the order of

182 10^{-5} yr^{-1}. We calculated the change in UVAI due to a change in surface reflectance of this order of

183 magnitude, and found that the change in UVAI was negligible. We also calculated the change in

184 UVAI due to changes in simulated aerosol altitude, but found that the trends in aerosol altitude

185 were negligible (order 10^{-5} hPa yr^{-1}). Therefore we focus our analysis on trends in aerosol

186 composition which have a larger effect on the UVAI as demonstrated below.

187   We use the GEOS-Chem model v11-01 (http://geos-chem.org) as input to the UVAI

188   simulation, and to calculate the sensitivity of the UVAI simulation to aerosol composition. The

189   simulation is driven by assimilated meteorological data from MERRA-2 Reanalysis of the NASA

190   Global Modeling and Assimilation Office (GMAO). Our simulation is conducted at a spatial

191   resolution of 2° x 2.5° with 47 vertical levels for the years 2005-2015. We supply VLIDORT with

192   GEOS-Chem aerosol fields coincident with OMI observations.

193   GEOS-Chem contains a detailed oxidant-aerosol chemical mechanism (Bey et al., 2001;

194   Park et al., 2004). The aerosol simulation includes the sulfate-nitrate-ammonium system

195   (Fountoukis and Nenes, 2007; Park et al., 2004; Pye et al., 2009), primary carbonaceous aerosol

196   (Park et al., 2003), mineral dust (Fairlie et al., 2007), and sea salt (Jaeglé et al., 2011). Semivolatile

197   primary organic carbon and secondary organic aerosol formation is described in Pye et al. (2010).

198   We update the original semi-volatile partitioning of secondary OA (SOA) formed from isoprene

199   with the irreversible uptake scheme in Marais et al. (2016). HNO_3 concentrations are reduced

200   following Heald et al. (2012). Aerosol optical properties are based on the Global Aerosol Data Set

201   (GADS) (Koepke et al., 1997) as originally implemented by Martin et al. (2003), with updates for

202   organics and secondary inorganics from aircraft observations (Drury et al., 2010), for mineral dust

203   (Lee et al., 2009; Ridley et al., 2012), and for absorbing brown carbon (Hammer et al., 2016). Here

204   we update the mineral dust optics at ultraviolet wavelengths using a refractive index that minimizes

205   the difference between the mean simulated and OMI UVAI values to allow focus on trends.

206   Aerosols are treated as externally mixed.

207   Anthropogenic emissions are from the EDGARv4.3.1 global inventory (Crippa et al., 2016)

208   with emissions overwritten in areas with regional inventories for the United States (NEI11;Travis

209   et al., 2016), Canada (CAC), Mexico (BRAVO; Kuhns et al., 2005), Europe (EMEP;

210   http://www.emep.int/), China (MEIC v1.2; Li et al., 2017a) and elsewhere in Asia (MIX; Li et al.,

211   2017a). Emissions from open fires for individual years from the GFED4 inventory (Giglio et al.,

212   2013) are included. The long-term concentrations from this simulation have been extensively

213   evaluated versus ground-based $PM_{2.5}$ composition measurements where available, and versus

214   satellite-derived $PM_{2.5}$ trends (Li et al., 2017b).

215   The Supplement evaluates trends in simulated SO_2, NO_2, and AOD versus satellite

216   retrievals from multiple instruments and algorithms. We find broad consistency between our

217   simulated NO_2 and SO_2 column trends with those from OMI (Figures S1 and S2). Our simulated

218 AOD trends are generally consistent with the trends in satellite AOD retrievals, except for positive

219 trends in AOD over western North America and near the Aral Sea in most retrieval products, and

220 a negative trend in AOD over Mongolia/Inner Mongolia in all retrieval products (Figure S3).

221   We filter our GEOS-Chem aerosol simulated fields based on the coincident OMI pixels,

222 which are regridded to the model resolution of 2° x 2.5°. This allows for the direct comparison

223 between our GEOS-Chem simulation and the OMI UVAI observations.

224

225 **3. Trend in emissions of GEOS-Chem aerosols and their precursors**

226   Figure 1 shows the trends in emissions of aerosols and their precursors from our GEOS-

227 Chem simulation calculated from the GLS regression of monthly time series values for 2005-2015.

228 Cool colors indicate negative trend values, warm colors indicate positive trend values, and the

229 opacity of the colors indicates the statistical significance of the trends. The trends in emissions of

230 sulfur dioxide (SO_2) and nitrogen oxides (NO_x) follow similar patterns (Figure 1a and 1b,

231 respectively). Negative trends (-1 to -0.01 kg km^{-2} yr^{-1}) are present over North America and

232 Europe, corresponding to pollution controls (Leibensperger et al., 2012; Klimont et al., 2013;

233 Curier et al., 2014; Simon et al., 2014; Xing et al., 2015; Li et al., 2017a). Positive trends (0.5 to 1

234 kg km^{-2} yr^{-1}) in both species are present over India and eastern China, however the positive trends

235 in emissions of SO_2 over eastern China are interspersed with negative trends (-1 to -0.5 kg km^{-2}

236 yr^{-1}) in SO_2 emissions, corresponding to the deployment of desulfurization equipment on power

237 plants in recent years (Lu et al., 2011; Klimont et al., 2013; Wang et al., 2015). Ammonia (NH_3)

238 emissions (Figure 1c) have positive trends (0.001 to 0.05 kg km^{-2} yr^{-1}) over most of South America,

239 North Africa, the Middle-East, and most of Asia with larger trends (0.1 to 0.5 kg km^{-2} yr^{-1}) over

240 India and eastern China. There are positive trends (0.001 to 0.05 kg km^{-2} yr^{-1}) in black carbon (BC)

241 emissions (Figure 1d) over North Africa, Europe, the Middle-East, India, and China, and negative

242 trends (-0.05 to -0.001 kg km^{-2} yr^{-1}) over North America, Europe, West Africa, and central South

243 America. The trends in primary organic aerosol (POA) emissions (Figure 1e) follow a similar

244 pattern as the trends in BC emissions, except there are negative trends (-0.1 to -0.05 kg km^{-2} yr^{-1})

245 over eastern China, and the negative trends (-1 to -0.1 kg km^{-2} yr^{-1}) over West Africa and central

246 South America are larger in magnitude reflecting regional changes in fire activity (Chen et al.,

247 2013; Andela and van der Werf, 2014). There are also positive trends (0.001 to 0.05 kg km^{-2} yr^{-1})

248 over the northern United States and Canada. The trends in dust emissions (Figure 1f) show the

249 largest magnitude of all the various species, although many have low statistical significance, with
250 areas of positive and negative trends (> 1 and < -1 kg km^{-2} yr^{-1}) over North Africa, positive trends
251 (> 1 kg km^{-2} yr^{-1}) parts of the Middle-East, and negative trends (< -1 kg km^{-2} yr^{-1}) over northern
252 China and southern Australia.
253
254 **4. Mean UVAI values for 2005-2015**
255 We examine the seasonal long-term mean UVAI values for insight into the spatial
256 distribution of the aerosol absorption signals. Figures 2 and 3 show the seasonal mean UVAI values
257 for 2005-2015 for OMI and the simulation, respectively. Positive UVAI values between 0.2 and
258 1.5 indicating aerosol absorption are present over major desert regions globally for both OMI and
259 the simulation, particularly over the Saharan, Iranian, and Thar deserts. These positive signals are
260 driven by the absorption by mineral dust (Herman et al., 1997; Torres et al., 1998; Buchard et al.,
261 2015). The simulation underestimates some of the smaller dust features captured by OMI, such as
262 over western North America, South America, Australia, and parts of Asia, perhaps reflecting an
263 underestimate in the simulated mineral dust lifetime (Ridley et al. 2012) and missing dust sources
264 (Ginoux et al., 2012; Guan et al., 2016; Huang et al., 2015; Philip et al., 2017). The seasonal
265 variation in the observed and simulated UVAI is similar albeit with larger simulated values in
266 spring (MAM) over North Africa. In all seasons, the UVAI values driven by absorption by dust in
267 the simulation are concentrated mostly over North Africa, while for OMI the UVAI values are
268 more homogeneous over the Middle-East and Asia as well. Positive UVAI values of ~0.2-1 over
269 West and central Africa appearing in both the OMI and simulated values correspond to absorption
270 by brown carbon from biomass burning activities in these regions (Jethva and Torres, 2011;
271 Hammer et al., 2016). Over ocean most data are removed by our strict cloud filter.
272
273 **5. Trend in UVAI values between 2005-2015**
274 Figure 4 shows the trend in OMI and simulated UVAI values (coincidently sampled from
275 OMI) calculated from the GLS regression of monthly UVAI time series values over 2005-2015.
276 Several regions exhibit consistency between the OMI and simulated UVAI trends. There are
277 statistically significant, positive trends in both OMI and simulated UVAI values over the eastern
278 United States (OMI: 1.0×10^{-5} to 2.5×10^{-4} yr^{-1}, simulated: 2.5×10^{-4} yr^{-1} to 5.0×10^{-4} yr^{-1}), and
279 Canada and parts of Russia (OMI: 1.0×10^{-5} to 2.5×10^{-4} yr^{-1}, simulated: 5.0×10^{-4} to 2.0×10^{-3} yr^{-1}).

280   Positive UVAI trends (1.0×10^{-5} to 2.5×10^{-4} yr^{-1}) in both OMI and simulated values are present

281   over Europe, although the simulated trends have low statistical significance. Statistically

282   significant, positive UVAI trends (5.0×10^{-4} to 2.0×10^{-3} yr^{-1}) in OMI values are apparent over

283   North Africa, which generally are captured by the simulation but with low statistical significance.

284   Negative UVAI trends (-1.5×10^{-3} yr^{-1} to -1.0×10^{-5} yr^{-1}) in both OMI and simulated values are

285   apparent over most of South America, southern Africa, and Australia. Negative UVAI trends ($-$

286   2×10^{-3} to -5.0×10^{-4} yr^{-1}) in both OMI and simulated values are present over West Africa, with low

287   statistical significance that could be related to the filtering of persistent clouds. OMI and simulated

288   UVAI values show negative trends (-2×10^{-3} to -5.0×10^{-4} yr^{-1}) over India, although the simulated

289   trends have lower statistical significance.

290   Some regions have trends in OMI UVAI values which are not captured by the simulation.

291   Statistically significant, positive UVAI trends (2.5×10^{-4} yr^{-1} to 1.5×10^{-3} yr^{-1}) over the western

292   United States are apparent in the OMI values but not in the simulation. Zhang et al. (2017) found

293   positive trends in aerosol absorption optical depth from OMI retrievals that they attributed to

294   positive trends in mineral dust over the region, which were not captured by their GEOS-Chem

295   simulation. Statistically significant, positive UVAI trends (5.0×10^{-4} to 2.0×10^{-3} yr^{-1}) in OMI

296   values exist over the Middle-East, while the simulation has negative trends with low statistical

297   significance. The OMI UVAI reveals a region of statistically significant, negative trends (-2×10^{-3}

298   to -5.0×10^{-4} yr^{-1}) over Mongolia/Inner Mongolia which is not captured by the simulation. There is

299   also a small area of statistically significant, positive UVAI trends (1.5×10^{-3} to 2.0×10^{-3} yr^{-1}) in

300   OMI values of over Central Asia between the Caspian Sea and the Aral Sea which is not captured

301   by the simulation. Trends in surface reflectance from the diminishing Aral Sea cannot solely

302   explain the UVAI trends since they extend over the Caspian Sea. Trends in mineral dust are a more

303   likely explanation as discussed further below.

304   Figures 5 and 6 show the seasonality of the OMI and simulated UVAI trends respectively.

305   The positive UVAI trends over the eastern United States is strongest in summer (JJA) for both

306   OMI and the simulation. The positive UVAI trends over North Africa and the Middle-East are

307   present for all seasons for OMI and for most seasons in the simulation, except in JJA for North

308   Africa and spring (MAM) for the Middle-East. The simulation underestimates the observed UVAI

309   trend over North Africa in SON, perhaps related to an underestimate in trends in mineral dust

310   emissions in the simulation during this season. He et al. (2014) examined the 2000-2010 trends in

311 global surface albedo using the Global Land Surface Satellites (GLASS) dataset and found no

312 significant trends over this region during SON. The negative trend in UVAI values over West

313 Africa is most apparent in the fall (SON) and winter (DJF) for both OMI and the simulation. The

314 negative OMI UVAI trends over Mongolia/Inner Mongolia and the positive OMI UVAI trends

315 near the Aral Sea are strongest in JJA and weakest in DJF, providing evidence for a mineral dust

316 source. The OMI UVAI trend over Mongolia/Inner Mongolia may be part of a longer term trend.

317 Guan et al. (2017) examined dust storm data over northern China (including Inner Mongolia) for

318 the period 1960-2007, and found that dust storm frequency has been declining over the region due

319 to a gradual decrease in wind speed. The current generation of chemical transport models is

320 unlikely to represent the source near the Aral Sea without an explicit parameterization of the drying

321 sea. The desiccation of the Aral Sea over recent decades has resulted in a steady decline in water

322 coverage over the area (Shi et al., 2014; Shi and Wang, 2015) and has led to the dried up sea bed

323 becoming an increasing source of dust activity in the region (Spivak et al., 2012). Indoitu et al.

324 (2015) found that most dust events are directed towards the west, consistent with the OMI

325 observations. An increase in surface reflectance due to the drying up of the sea bed could also

326 positively influence trends in UVAI. He et al. (2014) found a positive trend over 2000-2010 in

327 surface albedo over the region in JJA and SON, corresponding to when the OMI UVAI trends are

328 strongest.

329

6. Contribution of individual aerosol species to the simulated UVAI

331 To further interpret the UVAI trends, we examine the trends in aerosol concentrations from

332 our GEOS-Chem simulation (Figure 7). Figure 7a shows the trends in secondary inorganic aerosol

333 (SIA). There are statistically significant, negative trends over the eastern United States (-1 to -0.05

334 $\mu g\ m^{-2}\ yr^{-1}$) and statistically significant, positive trends over the Middle-East (0.05 to 0.5 $\mu g\ m^{-2}$

335 yr^{-1}), India (0.05 to 1 $\mu g\ m^{-2}\ yr^{-1}$), South America, and southern Africa (0.05 to 0.25 $\mu g\ m^{-2}\ yr^{-1}$).

336 Figure 7b shows the trends in dust. Similar to the trends in emissions, the trends in dust

337 concentrations are of the largest magnitude of the various species, however often with low

338 statistical significance. There are positive trends over the Middle-East (> 2 $\mu g\ m^{-2}\ yr^{-1}$), India (0.05

339 to 2 $\mu g\ m^{-2}\ yr^{-1}$), and north west China (1 to 2 $\mu g\ m^{-2}\ yr^{-1}$). There are also positive trends (0.05 to

340 0.25 $\mu g\ m^{-2}\ yr^{-1}$) with low statistical significance over the United States, northern South America,

341 southern Africa, and northern Australia. There is a combination of positive and negative trends (>

342 2 and < -2 µg m^{-2} yr^{-1}) over North Africa, and negative trends over China and Mongolia (< -2 µg

343 m^{-2} yr^{-1}) and Australia (-1 to -0.5 µg m^{-2} yr^{-1}). Figures 7c and 7d show the trends in total organic

344 aerosol (OA) and the absorbing brown carbon (BrC) component of OA, respectively. Positive

345 trends over Canada and parts of Russia (0.05 to 0.5 µg m^{-2} yr^{-1}) in total OA are mainly due to the

346 positive trend in BrC. Statistically significant, negative trends in total OA (-1 to -0.05 µg m^{-2} yr^{-1})

347 over the eastern United States are dominated by scattering organic aerosol. Statistically significant,

348 negative trends (-2 to -0.05 µg m^{-2} yr^{-1}) over West Africa and South America for total OA are

349 dominated by the trend in absorbing BrC. Figures 5e and 5f show the trends in black carbon (BC)

350 and salt, respectively. There are positive trends (0.05 to 0.25 µg m^{-2} yr^{-1}) in BC with low statistical

351 significance over India and China. Sea salt trends are negligible.

352   To gain further insight into how changes in aerosols effect the trends in simulated UVAI,

353 we examine the sensitivity of the UVAI to changes in individual aerosol species. Figure 8 shows

354 the change in annual mean UVAI due to doubling the concentration of individual aerosol species.

355 This information facilitates interpretation of the observed UVAI trends by identifying the chemical

356 components that could explain the observed trends. Doubling scattering SIA concentrations

357 (Figure 8a) decreases the UVAI between -0.25 and -0.1 over most of the globe, with the largest

358 changes over the Eastern United States, Europe, parts of the Middle-East, India, and south east

359 China. Doubling dust concentrations (Figure 8b) produces the largest changes in UVAI, causing

360 increases between 0.5 and 1 over North Africa, and smaller increases between 0.2 and 0.5 over the

361 Middle-East, Europe, and parts of Asia and Australia. Figures 8c and 8d show the changes in

362 UVAI due to doubling total OA concentrations and the absorbing BrC component, respectively.

363 The doubling of BrC increases the UVAI between 0.1 and 0.5 over Canada, West and central

364 Africa, India, parts of Russia, eastern China, and central South America. Doubling total OA

365 concentrations over central South America causes a net decrease of ~ -0.1 as the scattering

366 component of total OA cancels out the absorption by BrC. Doubling BC concentrations (Figure

367 8e) increases the UVAI of 0.1 over central Africa, India, and south east China, while doubling sea

368 salt concentrations (Figure 8f) has negligible effect on the UVAI.

369   Figure 9 shows the change in simulated UVAI due to the 2005-2015 trends in individual

370 aerosol species from our GEOS-Chem simulation. The change for each species is calculated by

371 applying the aerosol concentration trends for the individual aerosol type while leaving the

372 concentrations unchanged for the other aerosol species, then taking the difference between this

373   perturbed UVAI simulation and an unperturbed simulation. Negative trends in scattering SIA

374   (Figure 9a) increase the UVAI by 1.0×10^{-4} to 7.5×10^{-3} yr^{-1} over the eastern United States and by

375   1.0×10^{-4} to 2.5×10^{-3} yr^{-1} over Europe, corresponding to regions of positive UVAI trends in both

376   OMI and the simulation (Figure 4). Increasing SIA decreases the UVAI by -2.5×10^{-3} yr^{-1} to -

377   1.0×10^{-4} yr^{-1} over the Middle-East, India, and east China. Trends in dust concentrations (Figure

378   9b) cause the largest change in UVAI with regional increases $> 1 \times 10^{-2}$ yr^{-1} and regional decreases

379    $< -1 \times 10^{-2}$ yr^{-1}. Simulated UVAI trends due to mineral dust are mostly negative over North Africa,

380   East Asia, and Australia, while mostly positive over the Middle-East. Noisy trends in regional

381   meteorology cause heterogeneous trends in dust and in the UVAI, with low statistical significance.

382   Figures 9c and 9d show the change in UVAI due to the trends in total OA and the absorbing BrC

383   component of total OA, respectively. Most of the changes in UVAI due to the trends in total OA

384   are caused by the trends in the absorbing BrC component, with increases in the UVAI between

385   2.5×10^{-3} and 1×10^{-2} yr^{-1} over Canada and parts of Russia, corresponding to regions of positive

386   UVAI trends for both OMI and the simulation (Figure 4). There are decreases in the UVAI < -

387   1×10^{-2} yr^{-1} over central South America and West Africa due to the negative trends in BrC,

388   corresponding to regions of negative UVAI trends for both OMI and the simulation (Figure 4).

389   Over the eastern United States there is a mixture of increases and decreases in the UVAI due to

390   the trends in scattering organic aerosol. Positive trends in BC increase the UVAI (Figure 9e) by

391   1.0×10^{-4} to 2.5×10^{-3} yr^{-1} over India and China. There are no obvious changes in the UVAI due to

392   the trends in sea salt (Figure 9f).

393

394   **7. Conclusions**

395   Observations of aerosol scattering and absorption offer valuable information about aerosol

396   composition. We simulated the Ultraviolet Aerosol Index (UVAI), a method of detecting aerosol

397   absorption using satellite measurements, to interpret trends in OMI observed UVAI over 2005-

398   2015 to understand global trends in aerosol composition. We conducted our simulation using the

399   vector radiative transfer model VLIDORT with aerosol fields from the global chemical transport

400   model GEOS-Chem.

401   We examined the 2005-2015 trends in individual aerosol species from GEOS-Chem, and

402   applied these trends to the UVAI simulation to calculate the change in simulated UVAI due to the

403   trends in individual aerosol species. We found that global trends in the UVAI were largely

404 explained by trends in absorption by mineral dust, absorption by brown carbon, and scattering by
405 secondary inorganic aerosols. The two most prominent positive trends in the observed UVAI were
406 over North Africa and over Central Asia near the desiccating Aral Sea. The simulated UVAI
407 attributes the positive trends over North Africa to increasing mineral dust, despite an
408 underestimated simulated trend in fall (SON) that deserves further attention. The positive trends
409 in the observed UVAI over Central Asia near the shrinking Aral Sea are likely due to increased
410 dust emissions, a feature that is unlikely to be represented in most chemical transport models. The
411 most prominent negative trends in the observed UVAI were over East Asia, South Asia, and
412 Australia. The simulation attributed the negative trends over East Asia and Australia to decreasing
413 mineral dust, despite underestimating the trend in East Asia. The simulation attributed the negative
414 trend over South Asia to increasing scattering secondary inorganic aerosols, a trend that the
415 observations imply could be even larger. We found the positive trends in the UVAI over the eastern
416 United States that were strongest in summer (JJA) in both the observations and the simulation were
417 driven by negative trends in scattering secondary inorganic aerosol and organic aerosol. Observed
418 negative trends in winter (DJF) were less well simulated. Over West Africa and South America,
419 negative trends in UVAI were explained by negative trends in absorbing brown carbon. Thus,
420 trends in the observed UVAI offer valuable information on the evolution of global aerosol
421 composition that can be understood through quantitative simulation of the UVAI. Looking
422 forward, the availability of the UVAI observations from 1979 to the present offer a unique
423 opportunity to understand long-term trends in aerosol composition. The recent launch of the
424 TROPOspheric Monitoring Instrument (TROPOMI; Veefkind et al., 2012) and the forthcoming
425 geostationary constellation offer UVAI observations at finer spatial and temporal resolution. The
426 forthcoming Multi-Angle Imager for Aerosols (MAIA; Diner et al., 2018) satellite instrument
427 offers an exciting opportunity to derive even more information about aerosol composition by
428 combining measurements at ultraviolet wavelengths with multi-angle observations and
429 polarization sensitivity.
430
431
432
433
434

435 **Acknowledgements**

436 This work was supported by the Natural Science and Engineering Research Council of Canada

437 and the Killam Trusts. Computational facilities were provided in part by the Atlantic

438 Computational Excellence Network and the Graham consortiums of Compute Canada.

439

440

441

442

443

444

445

446

447

448

449

450

451

452

453

454

455

456

457

458

459

460

461

462

463

464

465

References

Andela, N. and van der Werf, G. R.: Recent trends in African fires driven by cropland expansion and El Niño to La Niña transition, Nat. Clim. Chang., 4(9), 791–795, doi:10.1038/nclimate2313, 2014.

Andreae, M. O. and Gelencsér, A.: Black carbon or brown carbon? The nature of light-absorbing carbonaceous aerosols, Atmos. Chem. Phys., 6(10), 3131–3148, doi:10.5194/acp-6-3131-2006, 2006.

Badarinath, K. V. S., Kharol, S. K., Kaskaoutis, D. G., Sharma, A. R., Ramaswamy, V. and Kambezidis, H. D.: Long-range transport of dust aerosols over the Arabian Sea and Indian region — A case study using satellite data and ground-based measurements, Glob. Planet. Change, 72(3), 164–181, doi:10.1016/j.gloplacha.2010.02.003, 2010.

Bey, I., Jacob, D. J., Yantosca, R. M., Logan, J. A., Field, B. D., Fiore, A. M., Li, Q., Liu, H. Y., Mickley, L. J. and Schultz, M. G.: Global modeling of tropospheric chemistry with assimilated meteorology: Model description and evaluation, J. Geophys. Res., 106(D19), 23073, doi:10.1029/2001JD000807, 2001.

Bond, T. C., Doherty, S. J., Fahey, D. W., Forster, P. M., Berntsen, T., DeAngelo, B. J., Flanner, M. G., Ghan, S., Kärcher, B., Koch, D., Kinne, S., Kondo, Y., Quinn, P. K., Sarofim, M. C., Schultz, M. G., Schulz, M., Venkataraman, C., Zhang, H., Zhang, S., Bellouin, N., Guttikunda, S. K., Hopke, P. K., Jacobson, M. Z., Kaiser, J. W., Klimont, Z., Lohmann, U., Schwarz, J. P., Shindell, D., Storelvmo, T., Warren, S. G. and Zender, C. S.: Bounding the role of black carbon in the climate system: A scientific assessment, J. Geophys. Res. Atmos., 118(11), 5380–5552, doi:10.1002/jgrd.50171, 2013.

Boys, B. L., Martin, R. V., van Donkelaar, A., MacDonell, R. J., Hsu, N. C., Cooper, M. J., Yantosca, R. M., Lu, Z., Streets, D. G., Zhang, Q. and Wang, S. W.: Fifteen-Year Global Time Series of Satellite-Derived Fine Particulate Matter, Environ. Sci. Technol., 48(19), 11109–11118, doi:10.1021/es502113p, 2014.

Buchard, V., da Silva, A. M., Colarco, P. R., Darmenov, A., Randles, C. A., Govindaraju, R., Torres, O., Campbell, J. and Spurr, R.: Using the OMI aerosol index and absorption aerosol optical depth to evaluate the NASA MERRA Aerosol Reanalysis, Atmos. Chem. Phys., 15(10), 5743–5760, doi:10.5194/acp-15-5743-2015, 2015.

Chen, Y., Morton, D. C., Jin, Y., Collatz, G. J., Kasibhatla, P. S., van der Werf, G. R., DeFries, R. S. and Randerson, J. T.: Long-term trends and interannual variability of forest, savanna and agricultural fires in South America, Carbon Manag., 4(6), 617–638, doi:10.4155/cmt.13.61, 2013.

Chin, M., Diehl, T., Tan, Q., Prospero, J. M., Kahn, R. A., Remer, L. A., Yu, H., Sayer, A. M., Bian, H., Geogdzhayev, I. V., Holben, B. N., Howell, S. G., Huebert, B. J., Hsu, N. C., Kim, D., Kucsera, T. L., Levy, R. C., Mishchenko, M. I., Pan, X., Quinn, P. K., Schuster, G. L., Streets, D. G., Strode, S. A., Torres, O. and Zhao, X.-P.: Multi-decadal aerosol variations from 1980 to 2009: a perspective from observations and a global model, Atmos. Chem. Phys., 14(7), 3657–3690, doi:10.5194/acp-14-3657-2014, 2014a.

Chin, M., Diehl, T., Tan, Q., Prospero, J. M., Kahn, R. A., Remer, L. A., Yu, H., Sayer, A. M., Bian, H., Geogdzhayev, I. V., Holben, B. N., Howell, S. G., Huebert, B. J., Hsu, N. C., Kim, D., Kucsera, T. L., Levy, R. C., Mishchenko, M. I., Pan, X., Quinn, P. K., Schuster, G. L., Streets, D.

508   G., Strode, S. A., Torres, O. and Zhao, X.-P.: Multi-decadal aerosol variations from 1980 to 2009:
509   a perspective from observations and a global model, Atmos. Chem. Phys., 14(7), 3657–3690,
510   doi:10.5194/acp-14-3657-2014, 2014b.

511   Crippa, M., Janssens-Maenhout, G., Dentener, F., Guizzardi, D., Sindelarova, K., Muntean, M.,
512   Van Dingenen, R. and Granier, C.: Forty years of improvements in European air quality: regional
513   policy-industry interactions with global impacts, Atmos. Chem. Phys., 16(6), 3825–3841,
514   doi:10.5194/acp-16-3825-2016, 2016.

515   Cui, H., Mao, P., Zhao, Y., Nielsen, C. P. and Zhang, J.: Patterns in atmospheric carbonaceous
516   aerosols in China: emission estimates and observed concentrations, Atmos. Chem. Phys., 15(15),
517   8657–8678, doi:10.5194/acp-15-8657-2015, 2015.

518   Curci, G., Hogrefe, C., Bianconi, R., Im, U., Balzarini, A., Baró, R., Brunner, D., Forkel, R.,
519   Giordano, L., Hirtl, M., Honzak, L., Jiménez-Guerrero, P., Knote, C., Langer, M., Makar, P. A.,
520   Pirovano, G., Pérez, J. L., San José, R., Syrakov, D., Tuccella, P., Werhahn, J., Wolke, R., Žabkar,
521   R., Zhang, J. and Galmarini, S.: Uncertainties of simulated aerosol optical properties induced by
522   assumptions on aerosol physical and chemical properties: An AQMEII-2 perspective, Atmos.
523   Environ., 115, 541–552, doi:10.1016/j.atmosenv.2014.09.009, 2015.

524   Curier, L., Kranenburg, R., Timmermans, R., Segers, A., Eskes, H. and Schaap, M.: Synergistic
525   Use of LOTOS-EUROS and NO2 Tropospheric Columns to Evaluate the NOX Emission Trends
526   Over Europe, pp. 239–245., 2014.

527   Deirmendjian, D.: Scattering and Polarization Properties of Water Clouds and Hazes in the Visible
528   and Infrared, Appl. Opt., 3(2), 187, doi:10.1364/AO.3.000187, 1964.

529   Dey, S. and Di Girolamo, L.: A decade of change in aerosol properties over the Indian
530   subcontinent, Geophys. Res. Lett., 38(14), n/a-n/a, doi:10.1029/2011GL048153, 2011.

531   Diner, D. J., Brauer, M., Bruegge, C., Burke, K. A., Chipman, R., Di Girolamo, L., Garay, M. J.,
532   Hasheminassab, S., Hyer, E., Jerrett, M., Jovanovic, V., Kalashnikova, O. V., Liu, Y., Lyapustin,
533   A. I., Martin, R. V., Nastan, A., Ostro, B. D., Ritz, B., Schwartz, J., Wang, J. and Xua, F.: Advances
534   in multiangle satellite remote sensing of speciated airborne particulate matter and association with
535   adverse health effects: from MISR to MAIA, J. Appl. Rem. Sens.., Submitted, 2018.

536   Drury, E., Jacob, D. J., Spurr, R. J. D., Wang, J., Shinozuka, Y., Anderson, B. E., Clarke, A. D.,
537   Dibb, J., McNaughton, C. and Weber, R.: Synthesis of satellite (MODIS), aircraft (ICARTT), and
538   surface (IMPROVE, EPA-AQS, AERONET) aerosol observations over eastern North America to
539   improve MODIS aerosol retrievals and constrain surface aerosol concentrations and sources, J.
540   Geophys. Res., 115(D14), D14204, doi:10.1029/2009JD012629, 2010.

541   Duncan, B. N., Martin, R. V., Staudt, A. C., Yevich, R. and Logan, J. A.: Interannual and seasonal
542   variability of biomass burning emissions constrained by satellite observations, J. Geophys. Res.,
543   108(D2), 4100, doi:10.1029/2002JD002378, 2003.

544   Fairlie, D. J., Jacob, D. J. and Park, R. J.: The impact of transpacific transport of mineral dust in
545   the United States, Atmos. Environ., 41(6), 1251–1266, doi:10.1016/j.atmosenv.2006.09.048,
546   2007.

547   Fioletov, V. E., McLinden, C. A., Krotkov, N., Li, C., Joiner, J., Theys, N., Carn, S. and Moran,
548   M. D.: A global catalogue of large SO2 sources and emissions derived from the Ozone Monitoring
549   Instrument, Atmos. Chem. Phys., 16(18), 11497–11519, doi:10.5194/acp-16-11497-2016, 2016.

Fountoukis, C. and Nenes, A.: ISORROPIA II: a computationally efficient thermodynamic equilibrium model for K^+–Ca^{2+}–Mg^{2+}–NH_4^+–Na^+–SO_4^{2-}–NO_3^-–Cl^-–H_2O aero, Atmos. Chem. Phys., 7(17), 4639–4659, doi:10.5194/acp-7-4639-2007, 2007.

Giglio, L., Randerson, J. T. and van der Werf, G. R.: Analysis of daily, monthly, and annual burned area using the fourth-generation global fire emissions database (GFED4), J. Geophys. Res. Biogeosciences, 118(1), 317–328, doi:10.1002/jgrg.20042, 2013.

Ginoux, P., Prospero, J. M., Gill, T. E., Hsu, N. C. and Zhao, M.: Global-scale attribution of anthropogenic and natural dust sources and their emission rates based on MODIS Deep Blue aerosol products, Rev. Geophys., 50(3), doi:10.1029/2012RG000388, 2012.

de Graaf, M., Stammes, P., Torres, O. and Koelemeijer, R. B. A.: Absorbing Aerosol Index: Sensitivity analysis, application to GOME and comparison with TOMS, J. Geophys. Res., 110(D1), D01201, doi:10.1029/2004JD005178, 2005.

Guan, H., Esswein, R., Lopez, J., Bergstrom, R., Warnock, A., Follette-Cook, M., Fromm, M. and Iraci, L. T.: A multi-decadal history of biomass burning plume heights identified using aerosol index measurements, Atmos. Chem. Phys., 10(14), 6461–6469, doi:10.5194/acp-10-6461-2010, 2010.

Guan, Q., Sun, X., Yang, J., Pan, B., Zhao, S., Wang, L., Guan, Q., Sun, X., Yang, J., Pan, B., Zhao, S. and Wang, L.: Dust Storms in Northern China: Long-Term Spatiotemporal Characteristics and Climate Controls, J. Clim., 30(17), 6683–6700, doi:10.1175/JCLI-D-16-0795.1, 2017.

Guan, X., Huang, J., Zhang, Y., Xie, Y. and Liu, J.: The relationship between anthropogenic dust and population over global semi-arid regions, Atmos. Chem. Phys., 16(8), 5159–5169, doi:10.5194/acp-16-5159-2016, 2016.

Guo, Y., Tian, B., Kahn, R. A., Kalashnikova, O., Wong, S. and Waliser, D. E.: Tropical Atlantic dust and smoke aerosol variations related to the Madden-Julian Oscillation in MODIS and MISR observations, J. Geophys. Res. Atmos., 118(10), 4947–4963, doi:10.1002/jgrd.50409, 2013.

Hammer, M. S., Martin, R. V., van Donkelaar, A., Buchard, V., Torres, O., Ridley, D. A. and Spurr, R. J. D.: Interpreting the ultraviolet aerosol index observed with the OMI satellite instrument to understand absorption by organic aerosols: implications for atmospheric oxidation and direct radiative effects, Atmos. Chem. Phys., 16(4), 2507–2523, doi:10.5194/acp-16-2507-2016, 2016.

He, T., Liang, S. and Song, D.-X.: Analysis of global land surface albedo climatology and spatial-temporal variation during 1981-2010 from multiple satellite products, J. Geophys. Res. Atmos., 119(17), 10,281-10,298, doi:10.1002/2014JD021667, 2014.

Heald, C. L., J. L. Collett Jr., J. L., Lee, T., Benedict, K. B., Schwandner, F. M., Li, Y., Clarisse, L., Hurtmans, D. R., Van Damme, M., Clerbaux, C., Coheur, P.-F., Philip, S., Martin, R. V. and Pye, H. O. T.: Atmospheric ammonia and particulate inorganic nitrogen over the United States, Atmos. Chem. Phys., 12(21), 10295–10312, doi:10.5194/acp-12-10295-2012, 2012.

Herman, J. R., Bhartia, P. K., Torres, O., Hsu, C., Seftor, C. and Celarier, E.: Global distribution of UV-absorbing aerosols from Nimbus 7/TOMS data, J. Geophys. Res., 102(D14), 16911, doi:10.1029/96JD03680, 1997.

Hsu, N. C., Gautam, R., Sayer, A. M., Bettenhausen, C., Li, C., Jeong, M. J., Tsay, S.-C. and Holben, B. N.: Global and regional trends of aerosol optical depth over land and ocean using SeaWiFS measurements from 1997 to 2010, Atmos. Chem. Phys. Atmos. Chem. Phys., 12, 8037–8053, doi:10.5194/acp-12-8037-2012, 2012.

Huang, J., Minnis, P., Yan, H., Yi, Y., Chen, B., Zhang, L. and Ayers, J. K.: Dust aerosol effect on semi-arid climate over Northwest China detected from A-Train satellite measurements, Atmos. Chem. Phys., 10(14), 6863–6872, doi:10.5194/acp-10-6863-2010, 2010.

Huang, J. P., Liu, J. J., Chen, B. and Nasiri, S. L.: Detection of anthropogenic dust using CALIPSO lidar measurements, Atmos. Chem. Phys., 15(20), 11653–11665, doi:10.5194/acp-15-11653-2015, 2015.

Indoitu, R., Kozhoridze, G., Batyrbaeva, M., Vitkovskaya, I., Orlovsky, N., Blumberg, D. and Orlovsky, L.: Dust emission and environmental changes in the dried bottom of the Aral Sea, Aeolian Res., 17, 101–115, doi:10.1016/j.aeolia.2015.02.004, 2015.

IPCC: Climate Change 2014: Impacts, Adaptation, and Vulnerability. Part A: Global and Sectoral Aspects. Contribution of Working Group II to the Fifth Assessment Report of the Intergovernmental Panel on Climate Change [Field, C.B., V.R. Barros, D.J. Dokken, K.J., Cambridge University Press, Cambridge, United Kingdom and New York, NY, USA., 2014.

Israelevich, P. L., Levin, Z., Joseph, J. H. and Ganor, E.: Desert aerosol transport in the Mediterranean region as inferred from the TOMS aerosol index, J. Geophys. Res. Atmos., 107(D21), AAC 13-1-AAC 13-13, doi:10.1029/2001JD002011, 2002.

Jaeglé, L., Quinn, P. K., Bates, T. S., Alexander, B. and Lin, J.-T.: Global distribution of sea salt aerosols: new constraints from in situ and remote sensing observations, Atmos. Chem. Phys., 11(7), 3137–3157, doi:10.5194/acp-11-3137-2011, 2011.

Jethva, H. and Torres, O.: Satellite-based evidence of wavelength-dependent aerosol absorption in biomass burning smoke inferred from Ozone Monitoring Instrument, Atmos. Chem. Phys., 11(20), 10541–10551, doi:10.5194/acp-11-10541-2011, 2011.

Kahn, R. A. and Gaitley, B. J.: An analysis of global aerosol type as retrieved by MISR, J. Geophys. Res. Atmos., 120(9), 4248–4281, doi:10.1002/2015JD023322, 2015.

Kalashnikova, O. V. and Kahn, R. A.: Mineral dust plume evolution over the Atlantic from MISR and MODIS aerosol retrievals, J. Geophys. Res., 113(D24), D24204, doi:10.1029/2008JD010083, 2008.

Kaskaoutis, D. G., Kharol, S. K., Sifakis, N., Nastos, P. T., Sharma, A. R., Badarinath, K. V. S. and Kambezidis, H. D.: Satellite monitoring of the biomass-burning aerosols during the wildfires of August 2007 in Greece: Climate implications, Atmos. Environ., 45(3), 716–726, doi:10.1016/j.atmosenv.2010.09.043, 2011.

Klimont, Z., Smith, S. J. and Cofala, J.: The last decade of global anthropogenic sulfur dioxide: 2000–2011 emissions, Environ. Res. Lett. Environ. Res. Lett, 8(8), 14003–6, doi:10.1088/1748-9326/8/1/014003, 2013.

Klimont, Z., Kupiainen, K., Heyes, C., Purohit, P., Cofala, J., Rafaj, P., Borken-Kleefeld, J. and Schöpp, W.: Global anthropogenic emissions of particulate matter including black carbon, Atmos. Chem. Phys., 17(14), 8681–8723, doi:10.5194/acp-17-8681-2017, 2017.

632 Koepke, P., Hess, M., Schult, I. and Shettle, E. P.: Global Aerosol Dataset, report, Max-Planck
633 Inst. fur Meteorol., Hamburg, Germany., 1997.

634 Kristiansen, N. I., Stohl, A., Olivié, D. J. L., Croft, B., Søvde, O. A., Klein, H., Christoudias, T.,
635 Kunkel, D., Leadbetter, S. J., Lee, Y. H., Zhang, K., Tsigaridis, K., Bergman, T., Evangeliou, N.,
636 Wang, H., Ma, P.-L., Easter, R. C., Rasch, P. J., Liu, X., Pitari, G., Di Genova, G., Zhao, S. Y.,
637 Balkanski, Y., Bauer, S. E., Faluvegi, G. S., Kokkola, H., Martin, R. V., Pierce, J. R., Schulz, M.,
638 Shindell, D., Tost, H. and Zhang, H.: Evaluation of observed and modelled aerosol lifetimes using
639 radioactive tracers of opportunity and an ensemble of 19 global models, Atmos. Chem. Phys.,
640 16(5), 3525–3561, doi:10.5194/acp-16-3525-2016, 2016.

641 Kuhns, H., Knipping, E. M. and Vukovich, J. M.: Development of a United States–Mexico
642 Emissions Inventory for the Big Bend Regional Aerosol and Visibility Observational (BRAVO)
643 Study, J. Air Waste Manage. Assoc., 55(5), 677–692, doi:10.1080/10473289.2005.10464648,
644 2005.

645 Lee, C., Martin, R. V., van Donkelaar, A., O'Byrne, G., Krotkov, N., Richter, A., Huey, L. G. and
646 Holloway, J. S.: Retrieval of vertical columns of sulfur dioxide from SCIAMACHY and OMI: Air
647 mass factor algorithm development, validation, and error analysis, J. Geophys. Res., 114(D22),
648 D22303, doi:10.1029/2009JD012123, 2009.

649 Leibensperger, E. M., Mickley, L. J., Jacob, D. J., Chen, W.-T., Seinfeld, J. H., Nenes, A., Adams,
650 P. J., Streets, D. G., Kumar, N. and Rind, D.: Climatic effects of 1950–2050 changes in US
651 anthropogenic aerosols − Part 2: Climate response, Atmos. Chem. Phys., 12(7), 3349–3362,
652 doi:10.5194/acp-12-3349-2012, 2012.

653 Li, C., Martin, R. V., van Donkelaar, A., Boys, B. L., Hammer, M. S., Xu, J.-W., Marais, E. A.,
654 Reff, A., Strum, M., Ridley, D. A., Crippa, M., Brauer, M. and Zhang, Q.: Trends in Chemical
655 Composition of Global and Regional Population-Weighted Fine Particulate Matter Estimated for
656 25 Years, Environ. Sci. Technol., acs.est.7b02530, doi:10.1021/acs.est.7b02530, 2017a.

657 Li, M., Zhang, Q., Kurokawa, J., Woo, J.-H., He, K., Lu, Z., Ohara, T., Song, Y., Streets, D. G.,
658 Carmichael, G. R., Cheng, Y., Hong, C., Huo, H., Jiang, X., Kang, S., Liu, F., Su, H. and Zheng,
659 B.: MIX: a mosaic Asian anthropogenic emission inventory under the international collaboration
660 framework of the MICS-Asia and HTAP, Atmos. Chem. Phys., 17(2), 935–963, doi:10.5194/acp-
661 17-935-2017, 2017b.

662 Liu, F., Zhang, Q., van der A, R. J., Zheng, B., Tong, D., Yan, L., Zheng, Y. and He, K.: Recent
663 reduction in NO_x emissions over China: synthesis of satellite observations and emission
664 inventories, Environ. Res. Lett., 11(11), 114002, doi:10.1088/1748-9326/11/11/114002, 2016.

665 Liu, Y., Koutrakis, P. and Kahn, R.: Estimating fine particulate matter component concentrations
666 and size distributions using satellite-retrieved fractional aerosol optical depth: part 1--method
667 development., J. Air Waste Manag. Assoc., 57(11), 1351–9 [online] Available from:
668 http://www.ncbi.nlm.nih.gov/pubmed/18069458 (Accessed 6 September 2017), 2007.

669 Lu, Z., Zhang, Q. and Streets, D. G.: Sulfur dioxide and primary carbonaceous aerosol emissions
670 in China and India, Atmos. Chem. Phys. Atmos. Chem. Phys., 11, 9839–9864, doi:10.5194/acp-
671 11-9839-2011, 2011.

672 Mann, M. E. and Emanuel, K. A.: Atlantic hurricane trends linked to climate change, Eos, Trans.
673 Am. Geophys. Union, 87(24), 233, doi:10.1029/2006EO240001, 2006.

674   Mao, K. B., Ma, Y., Xia, L., Chen, W. Y., Shen, X. Y., He, T. J. and Xu, T. R.: Global aerosol
675   change in the last decade: An analysis based on MODIS data, Atmos. Environ., 94, 680–686,
676   doi:10.1016/j.atmosenv.2014.04.053, 2014.

677   Marais, E. A., Jacob, D. J., Jimenez, J. L., Campuzano-Jost, P., Day, D. A., Hu, W., Krechmer, J.,
678   Zhu, L., Kim, P. S., Miller, C. C., Fisher, J. A., Travis, K., Yu, K., Hanisco, T. F., Wolfe, G. M.,
679   Arkinson, H. L., Pye, H. O. T., Froyd, K. D., Liao, J. and McNeill, V. F.: Aqueous-phase
680   mechanism for secondary organic aerosol formation from isoprene: application to the southeast
681   United States and co-benefit of SO₂ emission controls, Atmos. Chem.
682   Phys., 16(3), 1603–1618, doi:10.5194/acp-16-1603-2016, 2016.

683   Martin, R. V., Jacob, D. J., Yantosca, R. M., Chin, M. and Ginoux, P.: Global and regional
684   decreases in tropospheric oxidants from photochemical effects of aerosols, J. Geophys. Res.,
685   108(D3), 4097, doi:10.1029/2002JD002622, 2003.

686   Mauritsen, T.: Arctic climate change: Greenhouse warming unleashed, Nat. Geosci., 9(4), 271–
687   272, doi:10.1038/ngeo2677, 2016.

688   Mehta, M., Singh, R., Singh, A., Singh, N. and Anshumali: Recent global aerosol optical depth
689   variations and trends — A comparative study using MODIS and MISR level 3 datasets, Remote
690   Sens. Environ., 181, 137–150, doi:10.1016/j.rse.2016.04.004, 2016.

691   de Meij, A., Pozzer, A. and Lelieveld, J.: Trend analysis in aerosol optical depths and pollutant
692   emission estimates between 2000 and 2009, Atmos. Environ., 51, 75–85,
693   doi:10.1016/j.atmosenv.2012.01.059, 2012.

694   Mielonen, T., Portin, H., Komppula, M., Leskinen, A., Tamminen, J., Ialongo, I., Hakkarainen, J.,
695   Lehtinen, K. E. J. and Arola, A.: Biomass burning aerosols observed in Eastern Finland during the
696   Russian wildfires in summer 2010 – Part 2: Remote sensing, Atmos. Environ., 47, 279–287,
697   doi:10.1016/j.atmosenv.2011.07.016, 2012.

698   Moosmüller, H., Chakrabarty, R. K. and Arnott, W. P.: Aerosol light absorption and its
699   measurement: A review, J. Quant. Spectrosc. Radiat. Transf., 110(11), 844–878,
700   doi:10.1016/j.jqsrt.2009.02.035, 2009.

701   Park, R. J., Jacob, D. J., Chin, M. and Martin, R. V.: Sources of carbonaceous aerosols over the
702   United States and implications for natural visibility, J. Geophys. Res., 108(D12), 4355,
703   doi:10.1029/2002JD003190, 2003.

704   Park, R. J., Jacob, D. J., Field, B. D., Yantosca, R. M. and Chin, M.: Natural and transboundary
705   pollution influences on sulfate-nitrate-ammonium aerosols in the United States: Implications for
706   policy, J. Geophys. Res., 109(D15), D15204, doi:10.1029/2003JD004473, 2004.

707   Penning de Vries, M. J. M., Beirle, S. and Wagner, T.: UV Aerosol Indices from SCIAMACHY:
708   introducing the SCattering Index (SCI), Atmos. Chem. Phys., 9(24), 9555–9567, doi:10.5194/acp-
709   9-9555-2009, 2009.

710   Penning de Vries, M. J. M., Beirle, S., Hörmann, C., Kaiser, J. W., Stammes, P., Tilstra, L. G.,
711   Tuinder, O. N. E. and Wagner, T.: A global aerosol classification algorithm incorporating multiple
712   satellite data sets of aerosol and trace gas abundances, Atmos. Chem. Phys., 15(18), 10597–10618,
713   doi:10.5194/acp-15-10597-2015, 2015.

714   Philip, S., Martin, R. V, Snider, G., Weagle, C. L., van Donkelaar, A., Brauer, M., Henze, D. K.,

715   Klimont, Z., Venkataraman, C., Guttikunda, S. K. and Zhang, Q.: Anthropogenic fugitive,
716   combustion and industrial dust is a significant, underrepresented fine particulate matter source in
717   global atmospheric models, Environ. Res. Lett., 12(4), 44018, doi:10.1088/1748-9326/aa65a4,
718   2017.

719   Pöschl, U.: Atmospheric Aerosols: Composition, Transformation, Climate and Health Effects,
720   Angew. Chemie Int. Ed., 44(46), 7520–7540, doi:10.1002/anie.200501122, 2005.

721   Pye, H. O. T., Liao, H., Wu, S., Mickley, L. J., Jacob, D. J., Henze, D. K. and Seinfeld, J. H.:
722   Effect of changes in climate and emissions on future sulfate-nitrate-ammonium aerosol levels in
723   the United States, J. Geophys. Res., 114(D1), D01205, doi:10.1029/2008JD010701, 2009.

724   Pye, H. O. T., Chan, A. W. H., Barkley, M. P. and Seinfeld, J. H.: Global modeling of organic
725   aerosol: the importance of reactive nitrogen (NO_x and
726   NO_3), Atmos. Chem. Phys., 10(22), 11261–11276, doi:10.5194/acp-10-
727   11261-2010, 2010.

728   Ramanathan, V. and Carmichael, G.: Global and regional climate changes due to black carbon,
729   Nat. Geosci., 1(4), 221–227, doi:10.1038/ngeo156, 2008.

730   Ridley, D. A., Heald, C. L. and Ford, B.: North African dust export and deposition: A satellite and
731   model perspective, J. Geophys. Res., 117(D2), D02202, doi:10.1029/2011JD016794, 2012.

732   Schepanski, K., Tegen, I., Laurent, B., Heinold, B. and Macke, A.: A new Saharan dust source
733   activation frequency map derived from MSG-SEVIRI IR-channels, Geophys. Res. Lett., 34(18),
734   L18803, doi:10.1029/2007GL030168, 2007.

735   Scollo, S., Kahn, R. A., Nelson, D. L., Coltelli, M., Diner, D. J., Garay, M. J. and Realmuto, V. J.:
736   MISR observations of Etna volcanic plumes, J. Geophys. Res. Atmos., 117(D6), n/a-n/a,
737   doi:10.1029/2011JD016625, 2012.

738   Shao, Y., Klose, M. and Wyrwoll, K.-H.: Recent global dust trend and connections to climate
739   forcing, J. Geophys. Res. Atmos., 118(19), 11,107-11,118, doi:10.1002/jgrd.50836, 2013.

740   Shi, W. and Wang, M.: Decadal changes of water properties in the Aral Sea observed by MODIS-
741   Aqua, J. Geophys. Res. Ocean., 120(7), 4687–4708, doi:10.1002/2015JC010937, 2015.

742   Shi, W., Wang, M. and Guo, W.: Long-term hydrological changes of the Aral Sea observed by
743   satellites, J. Geophys. Res. Ocean., 119(6), 3313–3326, doi:10.1002/2014JC009988, 2014.

744   Simon, H., Reff, A., Wells, B., Xing, J. and Frank, N.: Ozone Trends Across the United States
745   over a Period of Decreasing NOx and VOC Emissions, 2014.

746   Spivak, L., Terechov, A., Vitkovskaya, I., Batyrbayeva, M. and Orlovsky, L.: Dynamics of Dust
747   Transfer from the Desiccated Aral Sea Bottom Analysed by Remote Sensing, pp. 97–106,
748   Springer, Berlin, Heidelberg., 2012.

749   Spurr, R. J. D.: VLIDORT: A linearized pseudo-spherical vector discrete ordinate radiative
750   transfer code for forward model and retrieval studies in multilayer multiple scattering media, J.
751   Quant. Spectrosc. Radiat. Transf., 102(2), 316–342, doi:10.1016/j.jqsrt.2006.05.005, 2006.

752   Stier, P., Seinfeld, J. H., Kinne, S. and Boucher, O.: Aerosol absorption and radiative forcing,
753   Atmos. Chem. Phys., 7(19), 5237–5261, doi:10.5194/acp-7-5237-2007, 2007.

754   Storelvmo, T., Leirvik, T., Lohmann, U., Phillips, P. C. B. and Wild, M.: Disentangling greenhouse

755 warming and aerosol cooling to reveal Earth's climate sensitivity, Nat. Geosci., 9(4), 286–289,
756 doi:10.1038/ngeo2670, 2016.

757 Torres, O., Bhartia, P. K., Herman, J. R., Ahmad, Z. and Gleason, J.: Derivation of aerosol
758 properties from satellite measurements of backscattered ultraviolet radiation: Theoretical basis, J.
759 Geophys. Res., 103(D14), 17099, doi:10.1029/98JD00900, 1998.

760 Torres, O., Tanskanen, A., Veihelmann, B., Ahn, C., Braak, R., Bhartia, P. K., Veefkind, P. and
761 Levelt, P.: Aerosols and surface UV products from Ozone Monitoring Instrument observations:
762 An overview, J. Geophys. Res., 112(D24), D24S47, doi:10.1029/2007JD008809, 2007.

763 Torres, O., Chen, Z., Jethva, H., Ahn, C., Freitas, S. R. and Bhartia, P. K.: OMI and MODIS
764 observations of the anomalous 2008–2009 Southern Hemisphere biomass burning seasons, Atmos.
765 Chem. Phys., 10(8), 3505–3513, doi:10.5194/acp-10-3505-2010, 2010.

766 Torres, O., Bhartia, P. K., Jethva, H. and Ahn, C.: Impact of the Ozone Monitoring Instrument
767 Row Anomaly on the Long-term Record of Aerosol Products, Atmos. Meas. Tech., 1–25,
768 doi:10.5194/amt-2017-429, 2018.

769 Travis, K. R., Jacob, D. J., Fisher, J. A., Kim, P. S., Marais, E. A., Zhu, L., Yu, K., Miller, C. C.,
770 Yantosca, R. M., Sulprizio, M. P., Thompson, A. M., Wennberg, P. O., Crounse, J. D., St. Clair,
771 J. M., Cohen, R. C., Laughner, J. L., Dibb, J. E., Hall, S. R., Ullmann, K., Wolfe, G. M., Pollack,
772 I. B., Peischl, J., Neuman, J. A. and Zhou, X.: Why do models overestimate surface ozone in the
773 Southeast United States?, Atmos. Chem. Phys., 16(21), 13561–13577, doi:10.5194/acp-16-13561-
774 2016, 2016.

775 Veefkind, J. P., Aben, I., McMullan, K., Förster, H., de Vries, J., Otter, G., Claas, J., Eskes, H. J.,
776 de Haan, J. F., Kleipool, Q., van Weele, M., Hasekamp, O., Hoogeveen, R., Landgraf, J., Snel, R.,
777 Tol, P., Ingmann, P., Voors, R., Kruizinga, B., Vink, R., Visser, H. and Levelt, P. F.: TROPOMI
778 on the ESA Sentinel-5 Precursor: A GMES mission for global observations of the atmospheric
779 composition for climate, air quality and ozone layer applications, Remote Sens. Environ., 120, 70–
780 83, doi:10.1016/J.RSE.2011.09.027, 2012.

781 Wang, S., Zhang, Q., Martin, R. V, Philip, S., Liu, F., Li, M., Jiang, X. and He, K.: Satellite
782 measurements oversee China's sulfur dioxide emission reductions from coal-fired power plants,
783 Environ. Res. Lett., 10(11), 114015, doi:10.1088/1748-9326/10/11/114015, 2015.

784 Xing, J., Mathur, R., Pleim, J., Hogrefe, C., Gan, C.-M., Wong, D. C., Wei, C., Gilliam, R. and
785 Pouliot, G.: Observations and modeling of air quality trends over 1990–2010 across the Northern
786 Hemisphere: China, the United States and Europe, Atmos. Chem. Phys., 15(5), 2723–2747,
787 doi:10.5194/acp-15-2723-2015, 2015.

788 Zhang, L., Henze, D. K., Grell, G. A., Torres, O., Jethva, H. and Lamsal, L. N.: What factors
789 control the trend of increasing AAOD over the United States in the last decade?, J. Geophys. Res.
790 Atmos., 122(3), 1797–1810, doi:10.1002/2016JD025472, 2017.

791 Zhao, B., Wang, S. X., Liu, H., Xu, J. Y., Fu, K., Klimont, Z., Hao, J. M., He, K. B., Cofala, J. and
792 Amann, M.: NO x emissions in China: historical trends and future perspectives, Atmos. Chem.
793 Phys, 13, 9869–9897, doi:10.5194/acp-13-9869-2013, 2013.

794
795
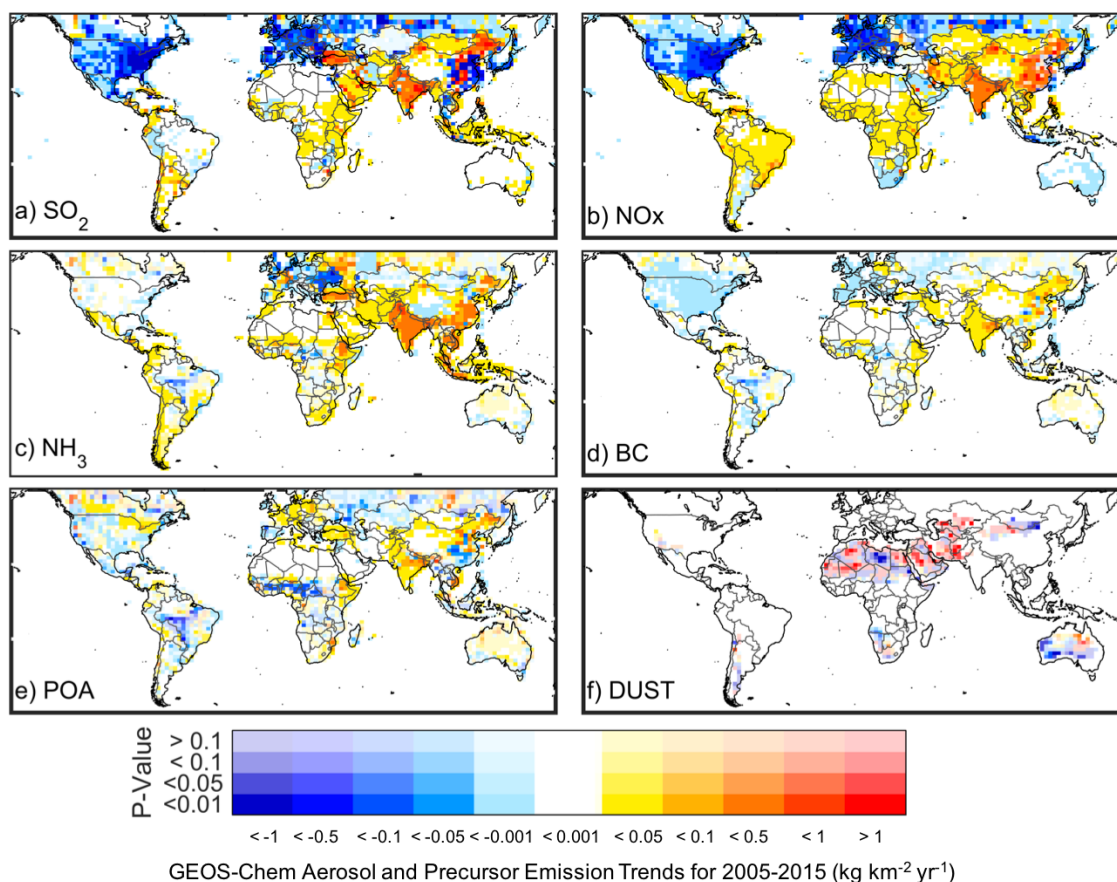
Figures

Figure 1: Trend in emissions of a) sulfur dioxide (SO_2) (kg SO_2 km^{-2} yr^{-1}), b) nitrogen oxides (NO_x) (kg NO km^{-2} yr^{-1}), ammonia (NH_3) (kg NH_3 km^{-2} yr^{-1}), black carbon (BC) (kg C km^{-2} yr^{-1}), primary organic carbon (POA) (kg C km^{-2} yr^{-1}), and dust (kg km^{-2} yr^{-1}) used in our GEOS-Chem simulation. The trends are calculated from the Generalized Least Squares regression of monthly time series values over 2005-2015.
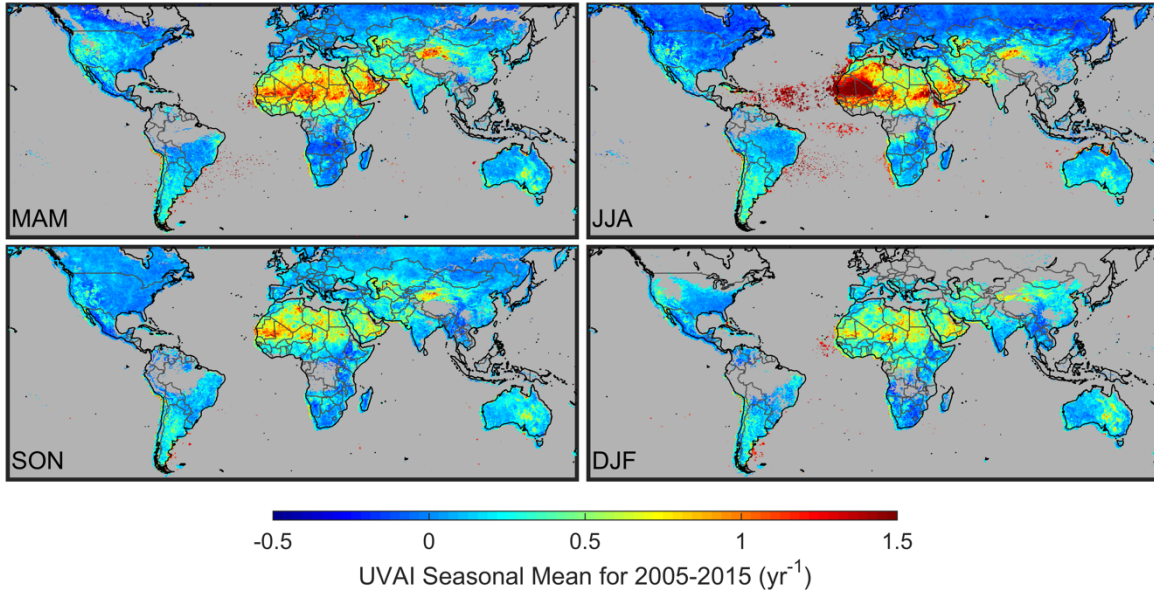
Figure 2: Seasonal mean UVAI values for the 2005-2015 period as observed by OMI for MAM (May, April, March), JJA (June, July August), SON (September, October, November), and DJF (December, January, February). Gray indicates persistent cloud fraction greater than 5%.

818
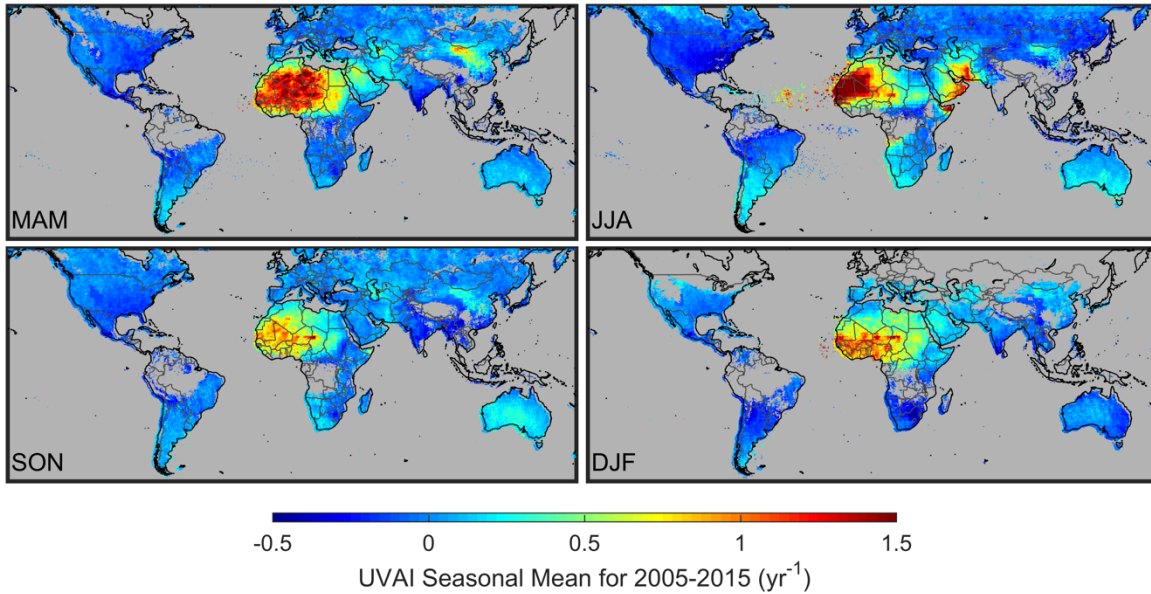
Figure 3: Seasonal mean UVAI values for the 2005-2015 period from our simulation coincidently sampled from OMI for MAM (May, April, March), JJA (June, July August), SON (September, October, November), and DJF (December, January, February). Gray indicates persistent cloud fraction greater than 5%.

823
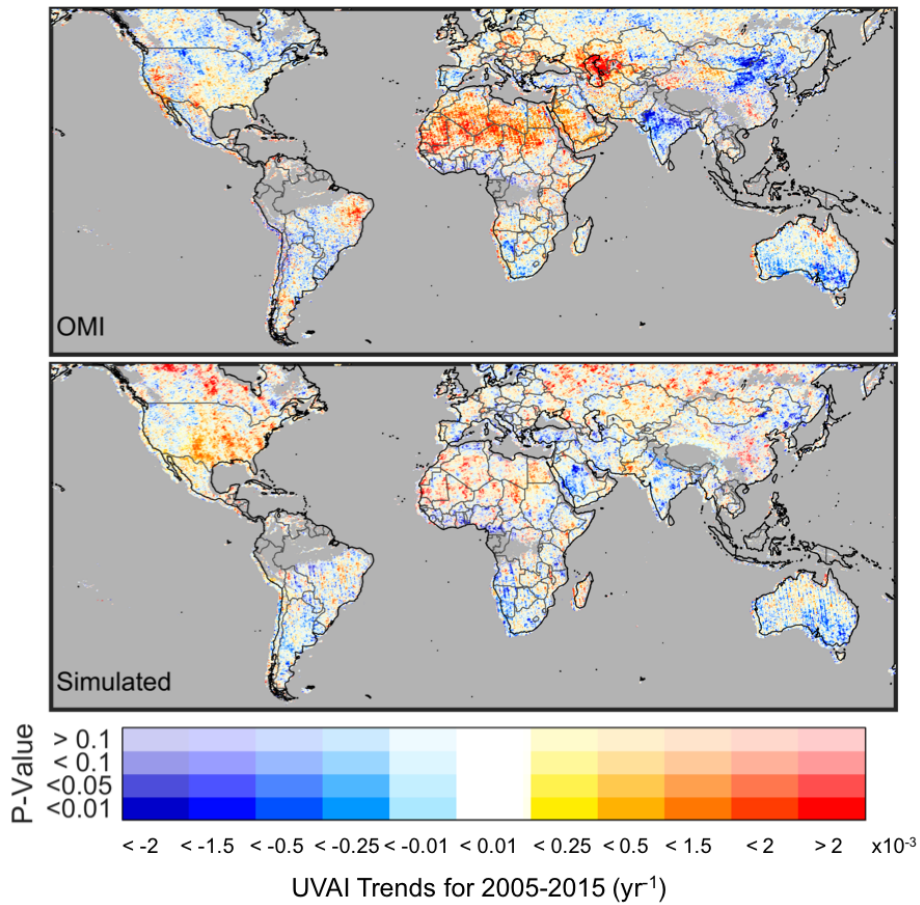
Figure 4: Trends in OMI (top panel) and simulated (bottom panel) UVAI values coincidently
sampled from OMI calculated from the Generalized Least Squares regression of monthly time
series values over 2005-2015. The opacity of the colors indicates the statistical significance of the
trend. Gray indicates persistent cloud fraction greater than 5%.

828
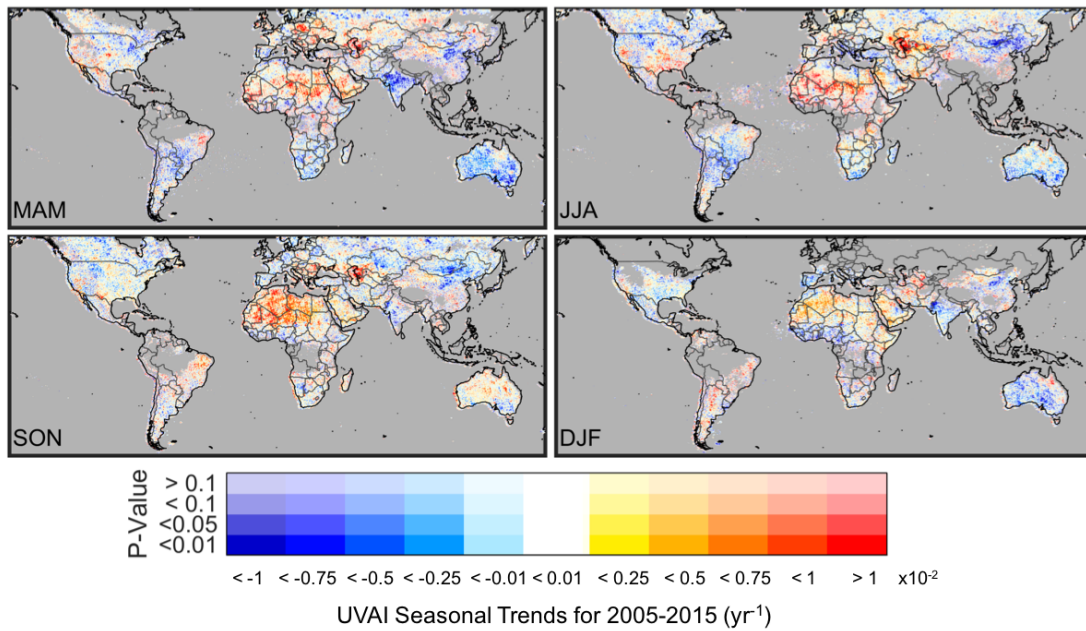
Figure 5: Seasonality of the trends in OMI UVAI values calculated from the Generalized Least Squares regression of monthly time series values over 2005-2015 for MAM (May, April, March), JJA (June, July August), SON (September, October, November), and DJF (December, January, February). The opacity of the colors indicates the statistical significance of the trend. Gray indicates persistent cloud fraction greater than 5%.

834
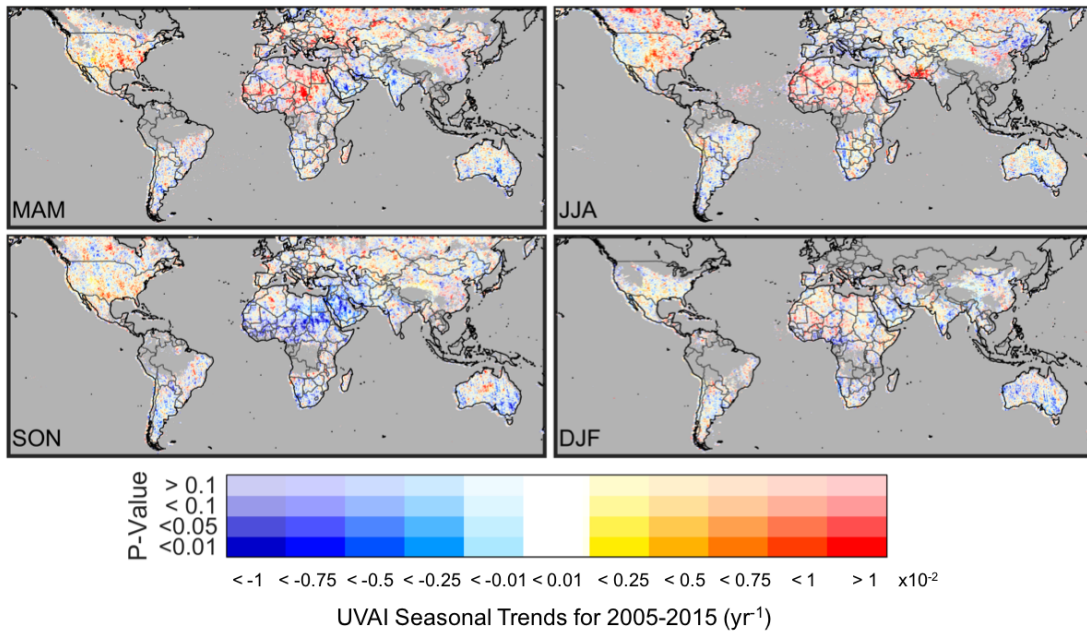
Figure 6: Seasonality of the trends in simulated UVAI values coincidently sampled from OMI calculated from the Generalized Least Squares regression of monthly time series values over 2005-2015 for MAM (May, April, March), JJA (June, July August), SON (September, October, November), and DJF (December, January, February). The opacity of the colors indicates the statistical significance of the trend. Gray indicates persistent cloud fraction greater than 5%.

840
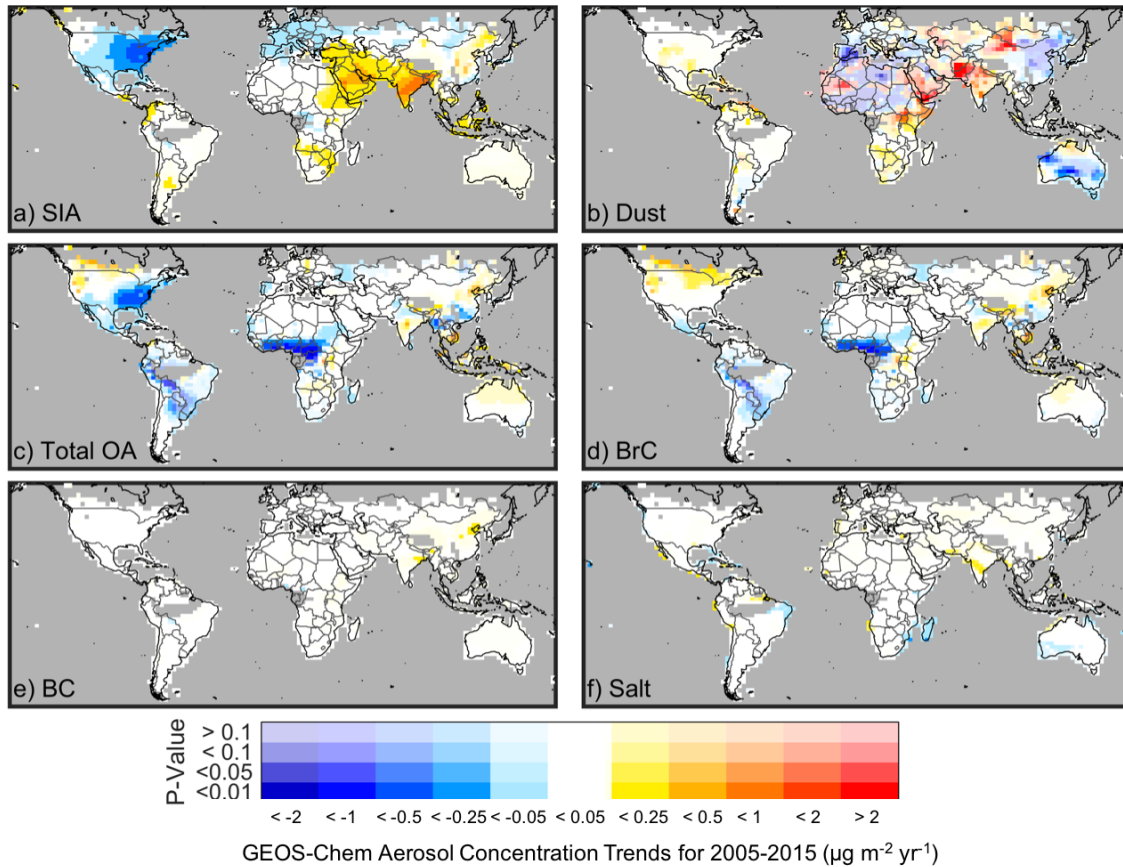
Figure 7: Trend in GEOS-Chem aerosol concentrations for a) secondary inorganic aerosol (SIA),
b) dust, c) total organic aerosol (OA), d) brown carbon (BrC), e) black carbon (BC), and f) sea
salt. The trends are calculated from the GLS regression of monthly aerosol concentration time
series values over 2005-2015. The opacity of the colors indicates the statistical significance of the
trend. Gray indicates persistent cloud fraction greater than 5%.

846
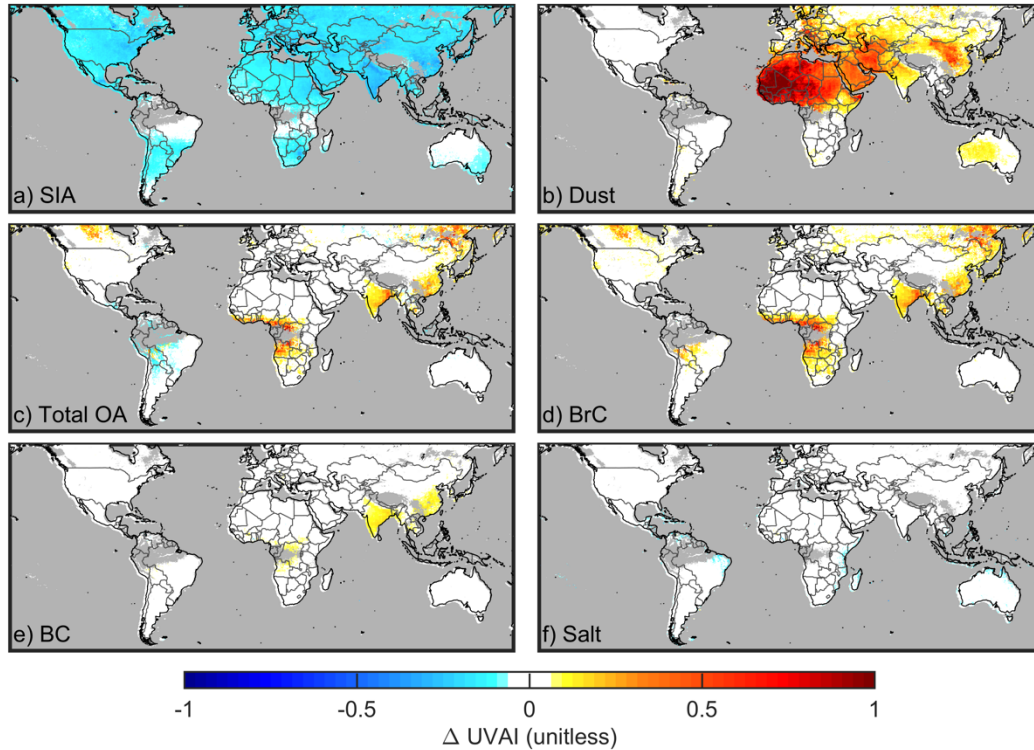
Figure 8: Annual mean change in simulated UVAI values for 2008 due to the doubling of concentrations of a) secondary inorganic aerosol (SIA), b) dust, c) total organic aerosol (OA), d) brown carbon (BrC), e) black carbon (BC), and f) sea salt from the GEOS-Chem simulation. Gray indicates persistent cloud fraction greater than 5%.
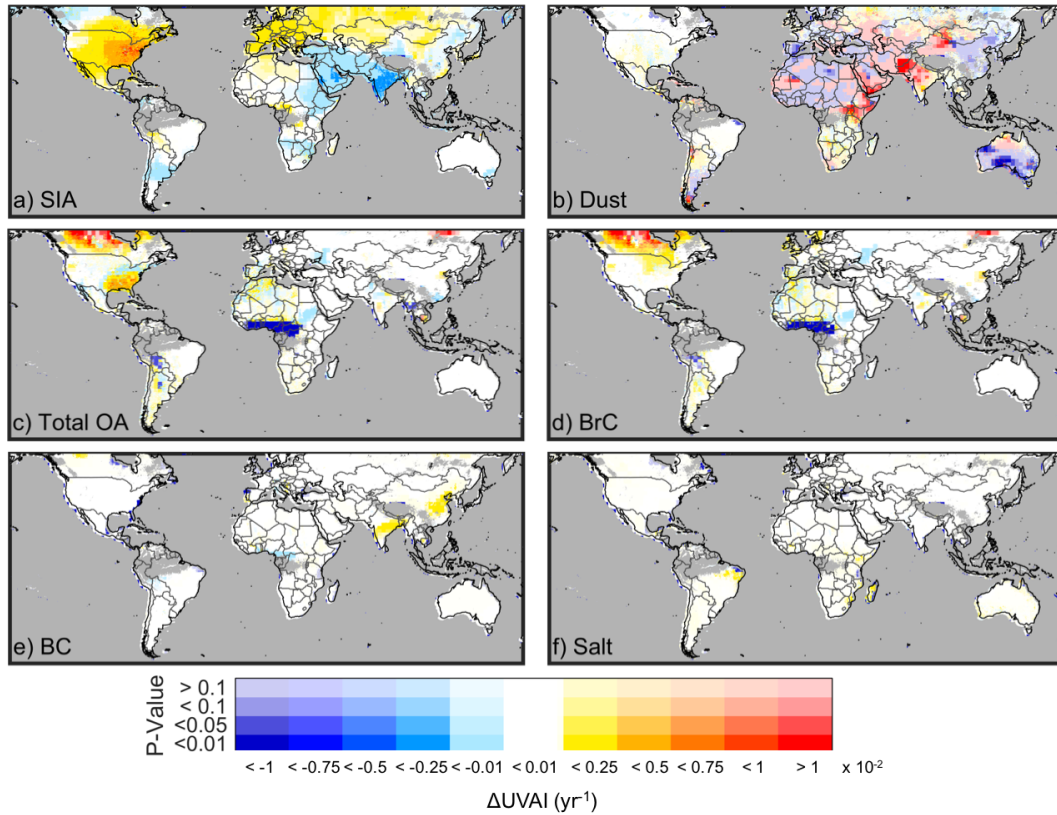
851

852 **Figure 9:** Change in simulated UVAI values due to the 2005-2015 trends in a) secondary inorganic
853 aerosols (SIA), b) dust, c) total organic aerosol (OA), d) brown carbon (BrC), e) black carbon
854 (BC), and f) sea salt from the GEOS-Chem simulation. Gray indicates persistent cloud fraction
855 greater than 5%.